UNIVERSITY OF LEEDS

This is a repository copy of *Model Anionic Block Copolymer Vesicles Provide Important Design Rules for Efficient Nanoparticle Occlusion within Calcite*.

White Rose Research Online URL for this paper:
http://eprints.whiterose.ac.uk/141036/

Version: Accepted Version

Article:
Ning, Y, Han, L, Derry, MJ et al. (2 more authors) (2019) Model Anionic Block Copolymer Vesicles Provide Important Design Rules for Efficient Nanoparticle Occlusion within Calcite. Journal of the American Chemical Society, 141 (6). pp. 2557-2567. ISSN 0002-7863

https://doi.org/10.1021/jacs.8b12507

Copyright © 2019 American Chemical Society. This document is the unedited Author's version of a Submitted Work that was subsequently accepted for publication in Journal of the American Chemical Society after peer review. To access the final edited and published work see http://doi.org/10.1021/jacs.8b12507.

Reuse
Items deposited in White Rose Research Online are protected by copyright, with all rights reserved unless indicated otherwise. They may be downloaded and/or printed for private study, or other acts as permitted by national copyright laws. The publisher or other rights holders may allow further reproduction and re-use of the full text version. This is indicated by the licence information on the White Rose Research Online record for the item.

Takedown
If you consider content in White Rose Research Online to be in breach of UK law, please notify us by emailing eprints@whiterose.ac.uk including the URL of the record and the reason for the withdrawal request.

White Rose university consortium
Universities of Leeds, Sheffield & York

eprints@whiterose.ac.uk
https://eprints.whiterose.ac.uk/

Model Anionic Block Copolymer Vesicles Provide Important Design Rules for Efficient Nanoparticle Occlusion within Calcite

Yin Ning,[*,†] Lijuan Han,[†] Matthew J. Derry,[†] Fiona C. Meldrum,[‡] and Steven P. Armes[*,†]

[†] Department of Chemistry, University of Sheffield, Brook Hill, Sheffield, South Yorkshire S3 7HF, U.K. E-mail: Y.Ning@sheffield.ac.uk; s.p.armes@sheffield.ac.uk.

[‡] School of Chemistry, University of Leeds, Woodhouse Lane, Leeds, LS2 9JT, U.K.

KEYWORDS: polymerization-induced self-assembly, block copolymer, vesicles, nanoparticle occlusion, calcite

ABSTRACT: Nanoparticle occlusion within growing crystals is of considerable interest because (i) it enhances our understanding of biomineralization and (ii) it offers a straightforward route for the preparation of novel nanocomposites. However, robust design rules for efficient occlusion remain elusive. Herein, we report the rational synthesis of a series of silica-loaded poly(glycerol monomethacrylate)-poly(2-hydroxypropyl methacrylate)-poly(ethylene glycol dimethacrylate)-poly(methacrylic acid) tetrablock copolymer vesicles using polymerization-induced self-assembly. The overall vesicle dimensions remain essentially constant for this series, hence systematic variation of the mean degree of polymerization (DP) of the anionic poly(methacrylic acid) steric stabilizer chains provides an unprecedented opportunity to investigate the design rules for efficient nanoparticle occlusion within host inorganic crystals such as calcite. Indeed, the stabilizer DP plays a decisive role in dictating both the extent of occlusion and the calcite crystal morphology: *sufficiently* long stabilizer chains are required to achieve extents of vesicle occlusion of up to 41 vol% but *overly* long stabilizer chains merely lead to significant changes in the crystal morphology, rather than promoting further occlusion. Furthermore, steric stabilizer chains comprising anionic carboxylate groups lead to superior occlusion performance compared to those composed of phosphate, sulfate or sulfonate groups. Moreover, occluded vesicles are subjected to substantial deformation forces, as shown by the significant change in shape after their occlusion. It is also demonstrated that such vesicles can act as 'Trojan Horses', enabling the occlusion of non-functional silica nanoparticles within calcite. In summary, this study provides important new physical insights regarding the efficient incorporation of guest nanoparticles within host inorganic crystals.

INTRODUCTION

Biominerals are composed of organic molecules and mineral hosts and can exhibit unique structures and remarkable mechanical properties.[1-8] Taking inspiration from this biogenic strategy, the occlusion of nanoparticle additives within inorganic crystal hosts has recently gained increasing attention.[9-15] Not only do such synthetic routes provide a straightforward approach to the rational design of new hybrid materials with enhanced physical properties such as hardness, magnetism, color or strong fluorescence,[16-20] but they can also inform our understanding of biomineralization processes.[21-24] There is no doubt that the nanoparticle surface chemistry dictates their occlusion.[25-27] However, the precise design rules required for efficient nanoparticle occlusion within inorganic crystals have not yet been elucidated. Appropriate surface functionality and optimal stabilizer surface density appear to be important parameters for optimizing the extent of nanoparticle occlusion.[28-29] However, progress in this area typically relies on empirical trial-and-error experiments. In this context, one important problem is the relative difficulty in synthesizing model nanoparticles that allow systematic variation of just one parameter (e.g. particle size, stabilizer surface density, stabilizer chain length, surface functionality, etc.). Conversely, if two or more parameters are varied simultaneously, it is almost impossible to reliably determine which parameter plays the more decisive role in determining the extent of nanoparticle occlusion.

There is considerable literature on block copolymer vesicles, not least because such vehicles can be used to encapsulate various cargoes by traditional post-polymerization processing techniques.[30-38] Polymerization-induced self-assembly (PISA) offers a particularly facile route to prepare block copolymer vesicles in a wide range of solvents at relatively high copolymer concentration.[39-47] Interestingly, this technique enables guest species (e.g. silica nanoparticles or enzymes) to be encapsulated *in situ* within the vesicle lumen *during the block copolymer synthesis*.[48-53] Recently, the synthesis of ABC triblock copolymer vesicles from AB diblock copolymer precursor vesicles has been reported.[54-58] For example, we have recently reported that framboidal/pH-responsive triblock copolymer vesicles can be prepared by growing

either poly(benzyl methacrylate) or poly(2-(diisopropylamino)ethyl methacrylate) as a third *hydrophobic* block.[54-55] Similarly, Yuan et al. investigated the effect of growing a hydrophobic block on the morphological evolution of diblock copolymer vesicles.[56-57] Of particular relevance to the present study, An et al. recently reported growth of a polyelectrolytic *hydrophilic* third block from cross-linked diblock copolymer 'seed' vesicles.[58] In principle, this approach enables the surface chemistry and electrophoretic behavior of such nano-objects to be readily tuned.

Inspired by this latter study, herein we design novel poly(glycerol monomethacrylate)$_{54}$-poly(2-hydroxypropyl methacrylate)$_{350}$-poly(ethylene glycol dimethacrylate)$_{25}$-poly(methacrylic acid)$_{x}$ tetrablock copolymer vesicles, within which silica nanoparticles can be readily encapsulated during their PISA synthesis via reversible addition-fragmentation chain transfer (RAFT) polymerization (see **Scheme 1**). These vesicles contain two types of stabilizer chains: non-ionic poly(glycerol monomethacrylate) and anionic poly(methacrylic acid) with the former block having a fixed degree of polymerization (DP) and the latter having a variable DP. The membrane-forming hydrophobic block comprises 2-hydroxypropyl methacrylate statistically copolymerized with a small amount of a dye label (fluorescein *O*-methacrylate). This block is then covalently cross-linked by the subsequent addition of ethylene glycol dimethacrylate to fix the dimensions of the precursor vesicles from which

a series of anionic stabilizer blocks of varying DP can be grown without disrupting the original vesicular morphology. For the sake of brevity, such tetrablock copolymers are denoted as G_{54}-H_{350}-E_{25}-MAA_x, where G, H, E and MAA represent poly(glycerol monomethacrylate), poly(2-hydroxypropyl methacrylate), poly(ethylene glycol dimethacrylate) and poly(methacrylic acid), respectively. The numerical subscripts indicate the fixed mean DP, while x represents the variable DP of the poly(methacrylic acid) block. In addition, the final poly(methacrylic acid) block can be readily replaced with poly(2-(phosphonooxy)ethyl methacrylate), poly(ammonium 2-sulfatoethyl methacrylate), poly(potassium 3-sulfopropyl methacrylate) or poly(sodium 4-styrenesulfonate), which are denoted as PEM, SEM, SPM and SS, respectively (see **Scheme 1**). Such model anionic vesicles offer an unprecedented opportunity to establish robust design rules for efficient nanoparticle occlusion within inorganic crystals by examining (i) the effect of systematically varying the DP and also (ii) the chemical nature of the anionic stabilizer in such experiments.

RESULTS AND DISCUSSION

Synthesis and Characterization of Silica-loaded G_{54}-H_{350}-E_{25}-MAA_x Vesicles. A non-ionic poly(glycerol monomethacrylate) macromolecular chain transfer agent (G macro-CTA) with a mean DP of 54 was synthesized in ethanol by using 4,4'-azobis(4-cyanovaleric acid) (ACVA) and (4-cyano-4-(phenylcarbonothioylthio)pentanoic acid) (CPCP) as initiator and RAFT chain transfer agent, respectively (see **Scheme 1**). Gel permeation chromatography (GPC) analysis of this macro-CTA indicated a number-average molecular weight (M_n) of 13,400 g mol^{-1}, with an M_w/M_n of 1.17 (see **Figure S1**). Moreover, this macro-CTA has a high blocking efficiency with minimal macro-CTA contamination, as indicated by comparison with the GPC curve obtained for a G_{54}-H_{350} diblock copolymer (see **Figure S1**). Subsequently, this macro-CTA was chain-extended via the statistical copolymerization of 2-hydroxypropyl methacrylate with fluorescein *O*-methacrylate (0.25 mol%) in the presence of silica nanoparticles (see **Scheme 1**). This PISA formulation leads to the formation of a concentrated aqueous dispersion of block copolymer vesicles: the silica nanoparticles are encapsulated *in situ* within the vesicle lumen while the fluorescent comonomer is co-located within the hydrophobic membrane-forming poly(2-hydroxypropyl methacrylate) (H_{350}) block. Approximately 99 % monomer conversion was achieved after 2.5 h at 70 °C as determined by ^{1}H NMR spectroscopy. Thereafter, ethylene glycol dimethacrylate was added to covalently cross-link the vesicle membrane (see **Scheme 1**). This second-stage polymerization was quenched after 4 h at 70 °C and excess, non-encapsulated silica nanoparticles were removed via six centrifugation-redispersion cycles (5,000 rpm, 30 min). Cross-linking the G_{54}-H_{350} vesicles ensures that the vesicular morphology is retained and also fixes the vesicle dimensions. Such covalent stabilization is essential, because *linear* G_{54}-H_{350} vesicles become unstable when chain-extended using methacrylic acid (see **Figures S2a** and **S2b**): introducing the hydrophilic poly(methacrylic acid) block significantly perturbs the fractional packing parameter of the block copolymer chains, resulting in gradual loss of the vesicle morphology.[59] Moreover, a certain minimum degree of cross-linking is required to confer effective covalent stabilization. Thus, using 15 ethylene glycol dimethacrylate units per copolymer chain proved to be insufficient to stabilize G_{54}-H_{350}-E_{15}-MAA_{150} vesicles (see **Figure S3**), whereas cross-linked G_{54}-H_{350}-E_{25} vesicles remained intact when chain-extended with 150 units of methacrylic acid (see **Figures S2c** and **S2d**).

Scanning electron microscopy (SEM) analysis (see **Figure 1**) confirmed a well-defined vesicular morphology for the silica-loaded G_{54}-H_{350}-E_{25} triblock copolymer, suggesting that the presence of

silica nanoparticles did not disrupt the PISA process. However, the presence of silica nanoparticles leads to a significant increase in the mean hydrodynamic vesicle diameter from 210 ± 63 nm to 374 ± 95 nm, as indicated by dynamic light scattering (DLS), see **Figure 2a** and **Figure S4**. Owing to the difference in electron density, TEM analysis enables clear visualization of the encapsulated silica nanoparticles within the vesicle lumen, with closer inspection suggesting a mean membrane thickness of 36 ± 5 nm (see inset in **Figure 1**). This value is consistent with that calculated from cryo-TEM images (see **Figure S5a**). Bearing in mind the refractory nature of silica, thermogravimetric analysis (TGA, see **Figure S6**) indicated a silica content of 17.1% w/w, with the corresponding silica encapsulation efficiency estimated to be 9.9% (see Supporting Information).

These silica-loaded cross-linked vesicles were further chain-extended using methacrylic acid, targeting various DPs (e.g., 25, 50, 100, 150, 200 or 300; see **Scheme 1**). In each case, more than 99% monomer conversion was confirmed by ^{1}H NMR spectroscopy. Unfortunately, GPC studies cannot be performed because these vesicles are covalently cross-linked. Instead, the aqueous supernatants obtained after centrifugation of these aqueous vesicle dispersions were analysed using aqueous GPC. This technique confirmed that the amount of free poly(methacylic acid) is negligible, suggesting that almost all of the methacrylic acid monomer is polymerized from the RAFT end-groups within the precursor G_{54}-H_{350}-E_{25} vesicles, rather than via conventional free radical polymerization in solution (**Figure S7**). DLS studies indicated that increasing the poly(methacrylic acid) DP led to a systematic increase in hydrodynamic diameter from 374 ± 95 nm for the silica-loaded G_{54}-H_{350}-E_{25} precursor vesicles up to 412 ± 108 nm for silica-loaded G_{54}-H_{350}-E_{25}-MAA_{300} vesicles (see **Figure 2a**). This is because the poly(methacrylic acid) stabilizer chains lead to a thicker coronal layer that contributes to the overall hydrodynamic diameter.[27, 29] Interestingly, the mean membrane thickness for the silica-loaded G_{54}-H_{350}-E_{25}-MAA_{300} vesicles is slightly greater than that for the silica-loaded G_{54}-H_{350}-E_{25} vesicles (37 nm vs. 40 nm, see cryo-TEM images in **Figure S5**). Presumably, the presence of the highly anionic poly(methacrylic acid) block leads to additional solvation of the vesicle membrane. Such a minor difference is not easily discernible using conventional TEM owing to dehydration effects during sample preparation (see **Figure S8**). Silica-loaded G_{54}-H_{350}-E_{25} vesicles exhibited a zeta potential of around -30 mV at pH 9, which is attributed to the carboxylic acid end-group located on the G_{54} stabilizer block.[60] As expected, introducing poly(methacrylic acid) chains resulted in a marked change in anionic character (zeta potential ~ -50 mV) under the same conditions. Importantly, a zeta potential of approximately -18 mV was observed in the presence of 1.5 mM Ca^{2+} ions (see **Figure 2b**), which corresponds to the conditions used for occlusion experiments (see later). This suggests that Ca^{2+} ions bind to the anionic poly(methacrylic acid) chains.[21] Covalent stabilization of the G_{54}-H_{350}-E_{25} precursor vesicles ensured that no change in the vesicle dimensions could occur when growing the poly(methacrylic acid) chains, other than the incremental increase in the stabilizer layer thickness noted above. Indeed, SEM analysis confirms this to be the case (see **Figure S8**). It is worth emphasizing that this approach overcomes an intrinsic limitation associated with PISA formulations: a relatively short stabilizer block is normally required in order to target the vesicle phase space, because relatively long stabilizer blocks invariably lead to the formation of kinetically-trapped spheres.[61]

In contrast, the strategy used herein enables the convenient preparation of vesicles with relatively long stabilizer chains. Moreover, it allows the incorporation of *polyelectrolytic* stabilizer blocks, which usually prevent vesicle formation in aqueous media because of strong inter-chain repulsion within the stabilizer corona. The latter point is critical for the present study, because anionic

stabilizer blocks are essential for efficient occlusion within calcite. It is also noteworthy that systematic variation of the stabilizer DP is not expected to affect the stabilizer surface density of the vesicles, whereas this is not true for conventional PISA syntheses. This is important, because this parameter is known to affect the extent of occlusion of sulfate-based block copolymer nano-objects.[29] So-called 'grafting from' and 'grafting to' strategies have been widely used to prepare sterically-stabilized inorganic nanoparticles, which could in principle also act as model anionic nanoparticles for occlusion studies.[62-63] However, the 'grafting from' method is relatively complex and time-consuming, while the 'grafting to' strategy inevitably leads to a reduction in surface chain density when utilizing longer polyelectrolytic chains.[64-65]

Occlusion of Silica-Loaded G_{54}-H_{350}-E_{25}-MAA_x Vesicles within Calcium Carbonate Crystals. Calcium carbonate ($CaCO_3$) crystals were precipitated at around pH 9 by exposing an aqueous solution containing 1.50 mM Ca^{2+} and 7.77 µM silica-loaded G_{54}-H_{350}-E_{25}-MAA_x vesicles to ammonium carbonate vapor at 20 °C for 24 h.[66-67] This fixed *molar* concentration means that the vesicle *number* concentration is constant, regardless of the poly(methacrylic acid) DP. Characteristic rhombohedral crystals were obtained in the absence of any vesicles (see **Figure S9**). **Figure 3** shows schematic cartoons depicting a series of silica-loaded G_{54}-H_{350}-E_{25}-MAA_x vesicles (see first column) along with optical microscopy (OM) and SEM images obtained for $CaCO_3$ crystals grown in the presence of such vesicles. Interestingly, a significant reduction in transparency (as judged by OM imaging) is observed for crystals precipitated in the presence of G_{54}-H_{350}-E_{25}-MAA_x vesicles when increasing x from 0 to 50 (**Figures 3a~3c**). Moreover, the crystals became completely opaque when precipitated in the presence of G_{54}-H_{350}-E_{25}-MAA_x vesicles for which x ≥ 100 (see **Figures 3d~3g**). Meanwhile, the crystal morphology was also affected on changing the poly(methacrylic acid) chain length. SEM studies demonstrate that the crystal morphology evolves from perfect rhombohedra (**Figures 3h~3i**), to rhombohedra with truncated edges and rough faces (**Figures 3j~3l**), to particles capped at the apex with three adjacent (104) faces (**Figures 3m~3n**). These changes reflect the differing interactions of the vesicles with the acute and obtuse steps on the exposed {104} faces.[68] According to these observations, longer poly(methacrylic acid) block chain lengths clearly have a profound influence on modifying the crystal surface morphology. This is reasonable since longer poly(methacrylic acid) chains are more flexible in molecular conformation and have more carboxylic acid units, which both facilitate interactions between the polymer chains and the step edges/kink sites of the growing crystal, inducing morphological changes.[69] Nevertheless, Raman spectroscopy studies confirm that the polymorph for each of these crystals is calcite, with characteristic bands being observed at 1088 cm^{-1} (ν_1), 712 cm^{-1} (ν_4), 281 cm^{-1} and 154 cm^{-1} (lattice modes) (see **Figure S10**).[70]

Direct evidence for successful vesicle occlusion within calcite crystals was obtained by visualizing cross-sections of randomly-fractured crystals (**Figures 3o-3u**), which were obtained by lightly pressing and twisting a flat glass slide placed on top of the crystals. For crystals precipitated in the presence of the silica-loaded G_{54}-H_{350}-E_{25} vesicles, no occlusion was observed (see **Figure 3o**). This important control experiment demonstrates that the non-ionic poly(glycerol monomethacrylate) stabilizer chains do not promote vesicle occlusion. Relatively few voids and vesicles were detected for calcite crystals prepared in the presence of silica-loaded G_{54}-H_{350}-E_{25}-MAA_{25} vesicles (**Figure 3p**). A higher density of voids and vesicles was observed when using silica-loaded G_{54}-H_{350}-E_{25}-MAA_{50} vesicles (**Figure 3q**). For silica-loaded G_{54}-H_{350}-E_{25}-MAA_x vesicles where x ≥ 100, numerous uniform voids were observed (**Figures 3r-3u**). The voids are attributed to vesicle break-up during the crystal fracture process. For a relatively short poly(methacrylic acid) block (x = 25), vesicle occlusion within

the $CaCO_3$ crystals is relatively rare. This is because these anionic stabilizer chains are too short to extend beyond the corona layer of non-ionic poly(glycerol monomethacrylate) chains, so the vesicles cannot effectively bind to the growing crystal surface. In contrast, for longer poly(methacrylic acid) blocks (x ≥ 100; see **Figures 3r-3u**) the void density is high and individual voids are invariably isolated from their neighbours, which suggests that the extent of vesicle occlusion is higher and vesicles remain colloidally stable throughout the occlusion process. The initial [-COOH]/[Ca^{2+}] molar ratios for G_{54}-H_{350}-E_{25}-MAA_{25} and G_{54}-H_{350}-E_{25}-MAA_{300} are 0.13 and 1.55, respectively. Thus, for a fixed initial Ca^{2+} concentration, vesicles with longer poly(methacrylic acid) blocks can bind more Ca^{2+} ions per stabilizer chain. Moreover, such stabilizer chains possess higher conformational entropy; this enables them to adopt more favourable conformations to interact with the growing crystal surface, which is a prerequisite for vesicle occlusion. Additional SEM images of these vesicle/calcite nanocomposites are shown in **Figures S11-S17.** Comparing the OM images (**Figures 3a-3g**) with the corresponding SEM images (**Figures 3o-3u**), it is clear that the change in transparency of crystals is closely correlated to the extent of vesicle occlusion (i.e. higher vesicle occlusion leads to more opaque crystals). This is attributed to the significant difference in refractive index between the guest vesicles and the inorganic host matrix, which leads to light scattering rather than transmittance.[71]

Evaluation of the Chemical Nature of the Anionic Stabilizer Chains. It is clear that surface chemistry dictates the extent of nanoparticle occlusion.[21, 25-26] However, as far as we are aware, there are no systematic studies of the effect of varying the surface functionality in the context of nanoparticle occlusion within calcite. Thus, we extended our study to include a range of alternative anionic stabilizer blocks. In principle, a series of surface-functionalized vesicles can be readily prepared by simply chain-extending silica-loaded G_{54}-H_{350}-E_{25} precursor vesicles with various alternative anionic monomers, as shown in **Scheme 1** and **Figure 4**. Aqueous electrophoresis studies indicate that all five types of silica-loaded anionic vesicles possess highly negative zeta potentials in the absence of calcium ions between pH 5 and pH 9 (see **Figure S18**). DLS analyses indicated that chain extension of silica-loaded G_{54}-H_{350}-E_{25} vesicles using any one of these four monomers leads to an increase in hydrodynamic diameter (**Figure S19a**) when targeting a DP of 300. Again, zeta potentials of approximately -20 mV for the resulting anionic vesicles in the presence of 1.50 mM [Ca^{2+}] were observed (see **Figure S19b**). In each case, growth of the polyelectrolytic stabilizer block does not affect the original vesicle morphology (see **Figure S20**). $CaCO_3$ crystals prepared in the presence of such anionic vesicles always maintained their characteristic rhombohedral morphology, as judged by both optical microscopy and SEM studies (see **Figures 4a-h**). However, the former technique indicated that only those crystals precipitated in the presence of silica-loaded G_{54}-H_{350}-E_{25}-PEM_{300} vesicles were opaque (**Figure 4a**) while the rest remained transparent (see **Figures 4b-4d**), suggesting little or no vesicle occlusion. Raman spectroscopy studies confirmed the formation of calcite for each of these experiments (see **Figure S21**). Examination of cross-sections of individual crystals confirmed that *only* the silica-loaded G_{54}-H_{350}-E_{25}-PEM_{300} vesicles were densely occluded. For the other three types of anionic stabilizers, only minimal vesicle occlusion was observed (see **Figures 4j-4l**). Further SEM images are provided in the Supporting Information (**Figures S22-S25**).

Extent of Vesicle Occlusion. The extent of vesicle occlusion was determined by thermogravimetric analysis (TGA, see **Figure S26**). Regardless of their chemical composition, empty vesicles were fully pyrolyzed on heating to 500 °C, while silica-loaded vesicles yielded incombustible residues owing to their inorganic cargo. In control experiments, pure calcite crystals decomposed to form CaO and CO_2 at around 800 °C. Silica-loaded vesicle-occluded calcite crystals began to decompose at around

300 °C owing to degradation of their copolymer component. In this case, the resulting incombustible residues were assumed to be CaO and silica. Thus, a lower residue indicated a higher extent of vesicle occlusion. Calculation of the extents of vesicle occlusion determined from these TGA data is provided in the Supporting Information. As shown in **Figure 5a**, the extent of G_{54}-H_{350}-E_{25}-MAA_x vesicle occlusion by mass increased monotonically, with a maximum extent of occlusion of approximately 7.8% being obtained for G_{54}-H_{350}-E_{25}-MAA_{150} vesicles. This indicates that longer stabilizer chains promote greater nanoparticle occlusion. Given that the densities of calcite and the vesicles are 2.71 and 1.26 g cm^{-3} respectively, this corresponds to ~41% by volume (see Supporting Information for calculation details).

According to the literature, extents of organic nanoparticle occlusion within calcite are invariably less than 30% by volume, most likely owing to insufficiently long anionic stabilizer blocks (DP < 73).[21, 25, 29] It is perhaps noteworthy that this is the first study to demonstrate that nanoparticles with a mean diameter of up to approximately 400 nm can be uniformly occluded within calcite.[12, 26] In principle, a longer poly(methacrylic acid) stabilizer DP should enable stronger vesicle binding to the growing crystal surface and hence lead to higher extents of vesicle occlusion. However, no further increase in the extent of occlusion was obtained for either G_{54}-H_{350}-E_{25}-MAA_{200} or G_{54}-H_{350}-E_{25}-MAA_{300} vesicles (see **Figure 5a**). This could be the result of mutual electrostatic repulsion between neighboring anionic vesicles preventing their close approach during occlusion. However, using longer poly(methacrylic acid) stabilizer blocks can significantly alter the crystal morphology (**Figures 3m** and **3n**).

The extent of G_{54}-H_{350}-E_{25}-PEM_{300} vesicle occlusion within calcite is 5.2% by mass (or 31% by volume, see **Figure 5b**). Poly(ammonium 2-sulfatoethyl methacrylate), poly(potassium 3-sulfopropyl methacrylate) and poly(sodium 4-styrenesulfonate) are highly anionic polyelectrolytes, which might be expected to exhibit similarly efficient occlusion. However, only relatively low levels of occlusion are observed for these three types of vesicles (see **Figures 4j-4l**). At first sight, this is rather surprising because both sulfate-functionalized diblock copolymer spheres and sulfonate-functionalized Fe_3O_4 nanoparticles have been previously incorporated within calcite.[29, 72] There are three likely reasons for the minimal occlusion levels observed in the present work. Firstly, the surface stabilizer density may not be optimal: we have recently shown that relatively low stabilizer densities lead to higher extents of occlusion for sulfate-functionalized diblock copolymer spheres.[29] Secondly, solubility product data for the corresponding calcium salts suggest that the Ca^{2+} binding affinity for carboxylic acids and phosphates should be stronger than that of sulfates and sulfonates.[73] Thus the former two functional groups bind more strongly to Ca^{2+}, which in turn facilitates vesicle occlusion within the calcite crystals via Ca^{2+} bridging between anionic carboxylate groups and anionic sites on the surface of the growing crystal. In addition, both the sulfate-functionalized spheres and sulfonate-functionalized nanoparticles used earlier were much smaller (~20 nm diameter)[29, 72] compared to the anionic vesicles of ~400 nm diameter examined in the present work.

Nonetheless, based on the above observations, silica-loaded G_{54}-H_{350}-E_{25}-MAA_x vesicles can be densely occluded within calcite if $x \geq 100$, suggesting that a sufficiently long anionic stabilizer block is required to ensure efficient nanoparticle occlusion. Under otherwise identical conditions, anionic carboxylate functionality leads to greater nanoparticle occlusion compared to phosphate, sulfate or sulfonate groups. This suggests stronger Ca^{2+} ion binding by this relatively weak polyacid block,

which facilitates more effective interaction between such vesicles and the surface of the growing calcite crystals, leading in turn to more efficient occlusion.

Vesicle Deformation During Occlusion. Comparison of SEM images obtained for cross-sectioned calcite crystals prepared in the presence of various anionic vesicles reveals some interesting differences (see **Figure 6**). In the case of silica-loaded G_{54}-H_{350}-E_{25}-MAA_{50}, compressed vesicles (see red arrows) and voids with irregular edges (see blue arrows) are observed (**Figure 6a**), indicating that significant deformation occurs during occlusion. However, only non-spherical voids are observed for G_{54}-H_{350}-E_{25}-MAA_x vesicles when $x \geq 100$, (see **Figures 3r-3u**, **Figure 6b**). This suggests that the former vesicles are subjected to strong compressive forces during occlusion. Recently, Cho et al. used *in situ* atomic force microscopy to demonstrate that anionic diblock copolymer micelles also experience some degree of deformation during occlusion within calcite.[22] The much bigger anionic vesicles used herein appear to be significantly more deformable than such micelles. The change in morphology observed for the occluded vesicles in the present study is likely to be related to their differing interactions with the growing crystal surface. For silica-loaded G_{54}-H_{350}-E_{25}-MAA_{50} vesicles, their anionic stabilizer blocks ensure vesicle occlusion but these chains interact only weakly with the host crystal. Following vesicle binding onto the growing crystal surface, the passing steps compress the adsorbed vesicles, leading to their significant deformation.[22] Because these relatively short stabilizer chains do not strongly interact with the $CaCO_3$ lattice, some of the occluded vesicles become detached from the fresh surface that is exposed during random fracture of the crystals (see red arrows in **Figure 6a)**. In contrast, silica-loaded G_{54}-H_{350}-E_{25}-MAA_x vesicles for which $x \geq 100$ can bind strongly at step edges and the relatively long anionic poly(methacrylic acid) stabilizer chains become engulfed by the subsequent propagating steps. This intimate interaction between the stabilizer chains and the growing crystal lattice minimizes vesicle deformation by offsetting the compression exerted by the growing steps during occlusion.[22] Therefore, such vesicles merely adopt an ellipsoidal morphology and are invariably cleaved during random fracture of the crystals. This explains why only voids were observed for the cross-section of the crystal, rather than highly deformed vesicles (see **Figure 6b**).

Examination of a cross-section parallel to the (104) face of calcite crystal containing silica-loaded G_{54}-H_{350}-E_{25}-MAA_{100} vesicles indicates that these voids are distinctly ellipsoidal, rather than spherical (see **Figure 6c**). Surprisingly, no discernible vesicle membrane was observed, suggesting that the growing calcite penetrates well within the vesicles. This observation is consistent with the above hypothesis that the stabilizer chains become entrapped within the crystal lattice. In striking contrast, vesicle membranes could be observed by SEM after occlusion of poly(methacrylic acid)-poly(benzyl methacrylate) vesicles within calcite.[26] This difference can be explained in terms of the differing hydrophobic character of the two membrane-forming blocks: poly(2-hydroxypropyl methacrylate) is substantially hydrated[74] and hence only weakly hydrophobic, which facilitates crystal growth well within the vesicle membrane. However, poly(benzyl methacrylate) is strongly hydrophobic, which minimizes crystal growth within such vesicle membranes.

Silica nanoparticles were discernible within the voids, as shown in the inset image for **Figure 6c**. In control experiments, silica nanoparticles alone are only very rarely occluded within calcite crystals (see **Figure S27**). This is as expected because only nanoparticles with appropriate surface chemistry can be efficiently occluded within inorganic crystals.[11, 25, 27, 29] Thus, efficient incorporation of these new anionic guest vesicles into growing inorganic host crystals in principle provides a *generic* route

to prepare nanocomposite crystals with a wide range of chemical compositions. In this sense, these vesicles act as a 'Trojan Horse' to enable efficient occlusion of nanoparticles within calcite, regardless of their surface chemistry. Given that these vesicles are readily prepared in concentrated aqueous solution, therefore, the present study provides an important complementary example to that of cargo-loaded poly(methacrylic acid)-poly(benzyl methacrylate) vesicles prepared in alcoholic media.[71] Finally, the efficient occlusion of fluorescein dye-labeled vesicles offers a facile new route to the preparation of highly fluorescent calcite crystals (see **Figure 6d**).

CONCLUSIONS

In summary, polymerization-induced self-assembly has been used for the rational design of a series of silica-loaded tetrablock copolymer vesicles with fixed dimensions (i.e. a constant lumen volume) and a variable mean degree of polymerization for the anionic stabilizer block. Such model vesicles offer an unprecedented opportunity to systematically investigate the effect of varying this parameter on the extent of occlusion of anionic organic nanoparticles within calcite. Indeed, the extent of occlusion is dictated by the DP of the anionic stabilizer block: there is an optimal chain length that ensures efficient occlusion while avoiding any significant change in the crystal morphology. Perhaps surprisingly, vesicles decorated with anionic carboxylate groups are occluded more efficiently within calcite compared to those exhibiting surface phosphate, sulfate or sulfonate groups. The significant morphological deformation observed for the occluded vesicles suggests that they experience significant compressive forces as they are engulfed by the growing calcite. Finally, such anionic vesicles can act as 'Trojan Horses' that enable water-borne *non-functionalized* nanoparticles to be delivered within host inorganic crystals. This study provides important new insights regarding the design rules that govern the efficient occlusion of organic nanoparticles within inorganic crystals.

ASSOCIATED CONTENT

Supporting Information. Experimental details and characterization methods, GPC data, DLS size distributions, aqueous electrophoresis data, Raman spectra, TGA curves, additional SEM, TEM and cryo-TEM images. This material is available free of charge via the Internet at http://pubs.acs.org.

AUTHOR INFORMATION

Corresponding Author

*Y.Ning@sheffield.ac.uk (Y.N.)

*s.p.armes@sheffield.ac.uk (S.P.A.)

ORCID

Yin Ning: 0000-0003-1808-3513

Steven P. Armes: 0000-0002-8289-6351

Notes

The authors declare no competing financial interest.

ACKNOWLEDGMENT

EPSRC (EP/P005241/1) is thanked for post-doctoral support for Y.N., the Leverhulme Trust (RPG-2016-330) is thanked for post-doctoral support for M.J.D. and S.P.A. acknowledges a five-year ERC Advanced Investigator grant (PISA 320372) and an EPSRC Established Career Particle Technology Fellowship (EP/R003009/1). Dr. Svetomir B. Tzokov is thanked for his kind assistance with the cryo-TEM studies.

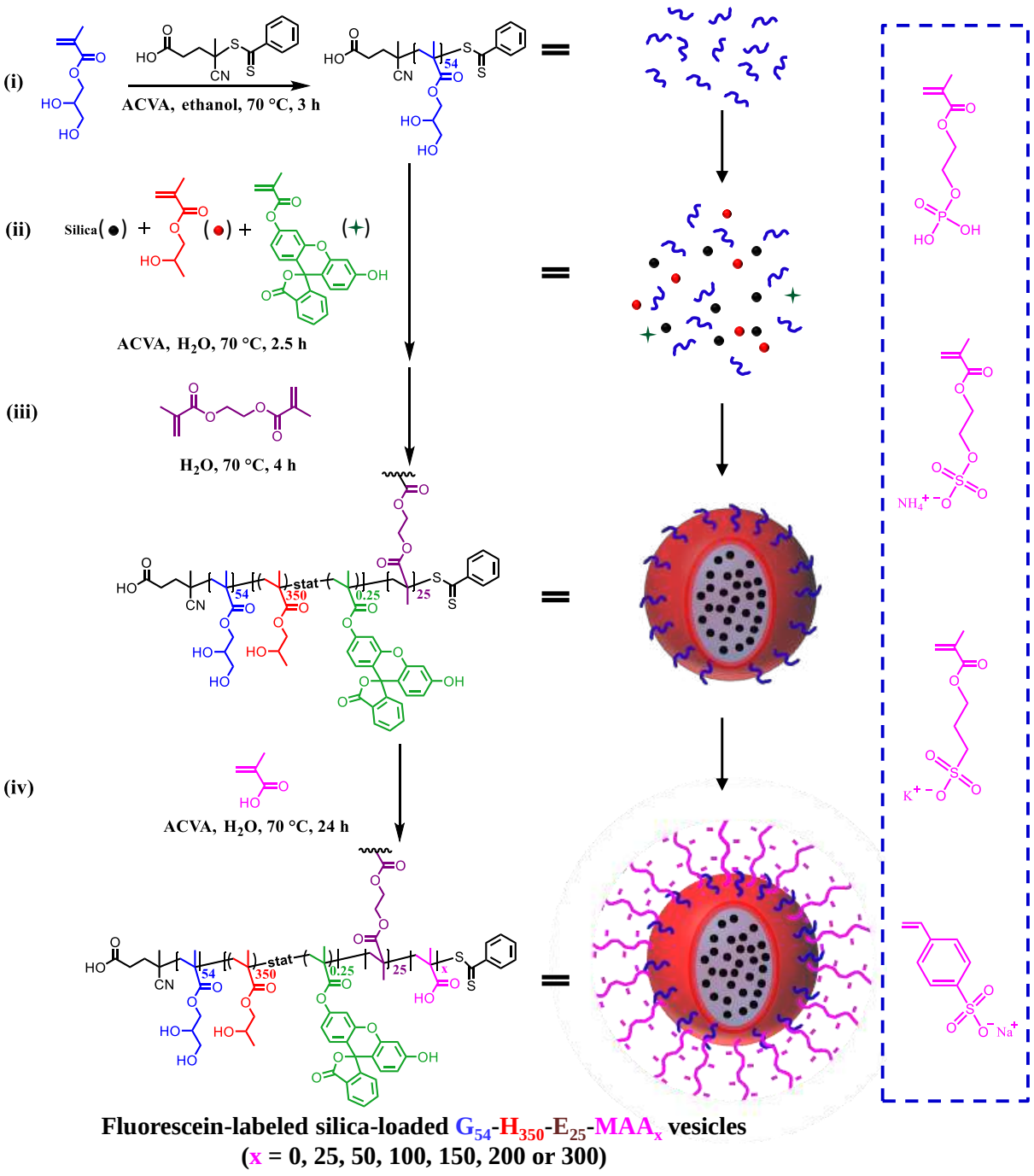

Scheme 1. Synthesis of silica-loaded, fluorescein-labeled poly(glycerol monomethacrylate)$_{54}$-poly(2-hydroxypropyl methacrylate)$_{350}$-poly(ethylene glycol dimethacrylate)$_{25}$-poly(methacrylic acid)$_x$ (G_{54}-H_{350}-E_{25}-MAA_x) vesicles: (i) synthesis of G_{54} macro-CTA via RAFT solution polymerization of glycerol monomethacrylate in ethanol; (ii) *in situ* encapsulation of silica nanoparticles during the statistical copolymerization of 2-hydroxypropyl methacrylate with 0.25 mol% fluorescein *O*-methacrylate to form G_{54}-H_{350} vesicles at 10% w/w solids via polymerization-induced self-assembly (PISA) in the presence of a 25% w/w aqueous dispersion of an 18 nm commercial silica sol; (iii) covalent cross-linking of linear G_{54}-H_{350} vesicles using ethylene glycol dimethacrylate; (iv) chain extension of cross-linked silica-loaded G_{54}-H_{350}-E_{25} vesicles using varying amounts of methacrylic acid (where x is the target degree of polymerization of the poly(methacrylic acid) block). Schematic cartoons depict the corresponding colloidal species that are present at each stage. Alternatively, methacrylic acid can be

replaced with one of four other anionic monomers (see dotted rectangle) to produce vesicles with surface phosphate, sulfate, aliphatic sulfonate or aromatic sulfonate groups.

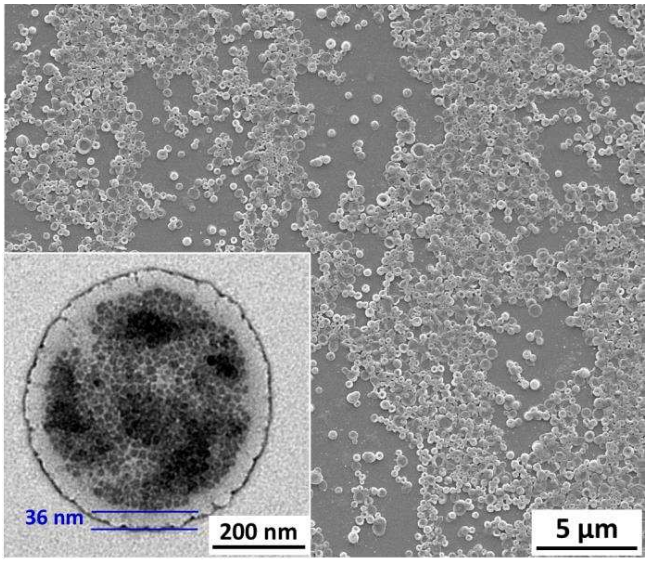

Figure 1. Scanning electron microscopy (SEM) image of silica-loaded G_{54}-H_{350}-E_{25} vesicles. Inset shows a representative transmission electron microscopy (TEM) image of a single silica-loaded G_{54}-H_{350}-E_{25} vesicle with a vesicle membrane thickness of 36 nm. The encapsulated 18 nm diameter silica nanoparticles are clearly discernible within the vesicle lumen.

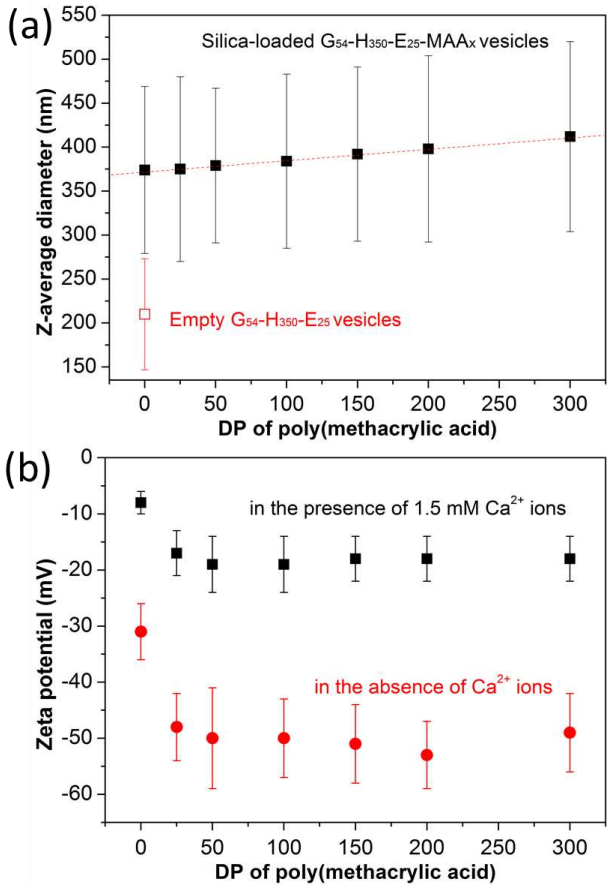

Figure 2. Dynamic light scattering (DLS) and aqueous electrophoresis data obtained for ~0.1% w/w aqueous dispersions of various vesicles: (a) z-average hydrodynamic diameter obtained in the presence of 1.5 mM [Ca^{2+}]. The red open square indicates the z-average hydrodynamic diameter for G_{54}-H_{350}-E_{25} vesicles prepared in the absence of any silica nanoparticles; (b) zeta potential vs. poly(methacrylic acid) block DPs (where x = 0, 25, 50, 100, 150, 200 or 300) measured in the presence (black squares) or absence (red spheres) of 1.5 mM [Ca^{2+}] at pH 9. The error bars in each Figure indicate standard deviations, rather than the experimental error.

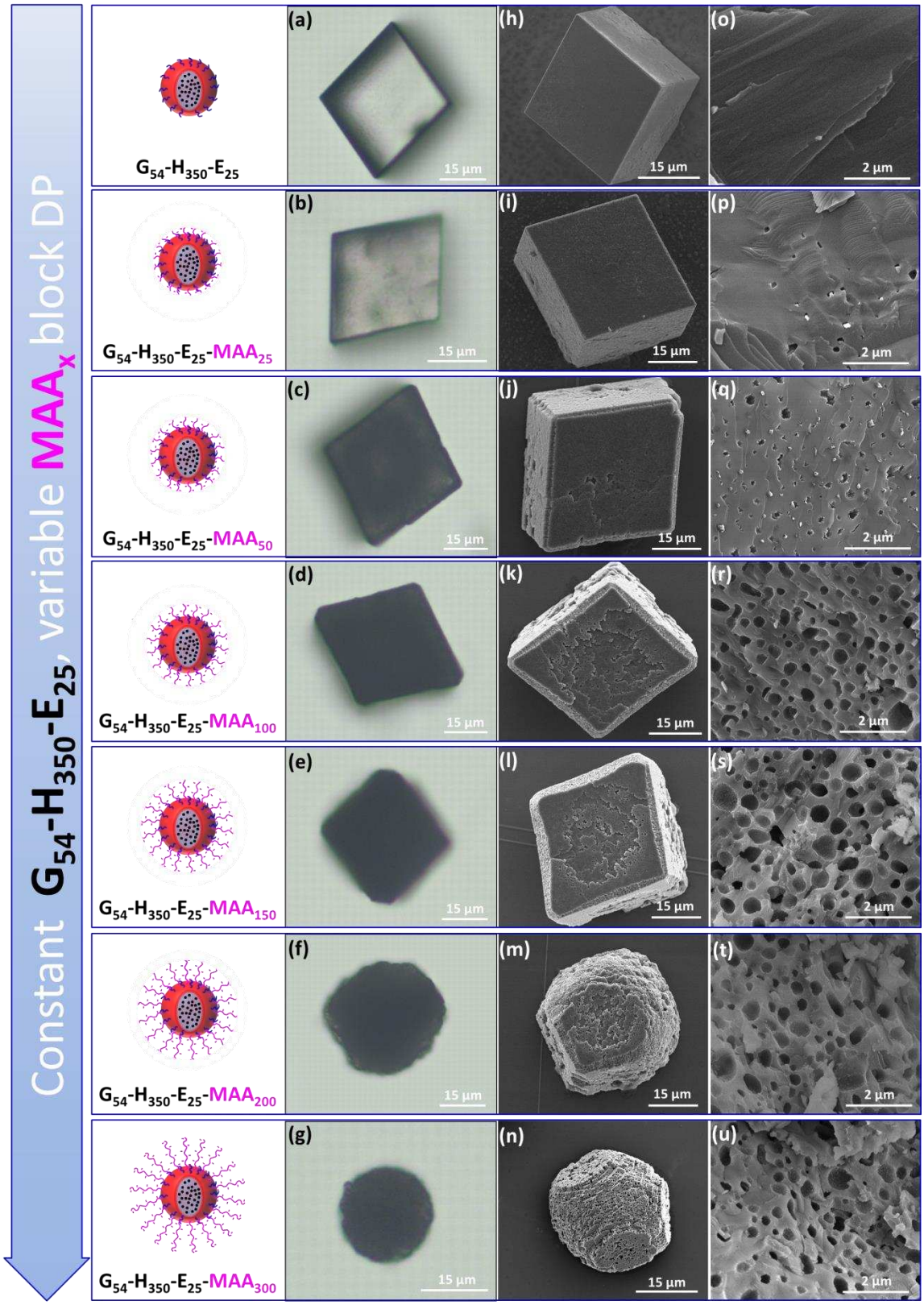

Figure 3. Effects of varying the target DP for the poly(methacrylic acid) stabilizer chains on the $CaCO_3$ crystal morphology and extent of vesicle occlusion. Schematic cartoons (see first column) representing a series of G_{54}-H_{350}-E_{25}-MAA_x vesicles with varying poly(methacrylic acid) block DPs (x = 0, 25, 50, 100, 150, 200 or 300); (a)-(g) representative optical microscopy (OM) images of $CaCO_3$ crystals precipitated in the presence of G_{54}-H_{350}-E_{25}-MAA_x vesicles; (h)-(n) representative SEM images

of the corresponding intact $CaCO_3$ crystals; (o)-(u) representative SEM images indicating the internal structure of randomly-fractured $CaCO_3$ crystals precipitated in the presence of corresponding G_{54}-H_{350}-E_{25}-MAA_x vesicles. [N.B. In all experiments, $CaCO_3$ crystals were precipitated in the presence of 1.50 mM $CaCl_2$ and 7.77 µM vesicles.]

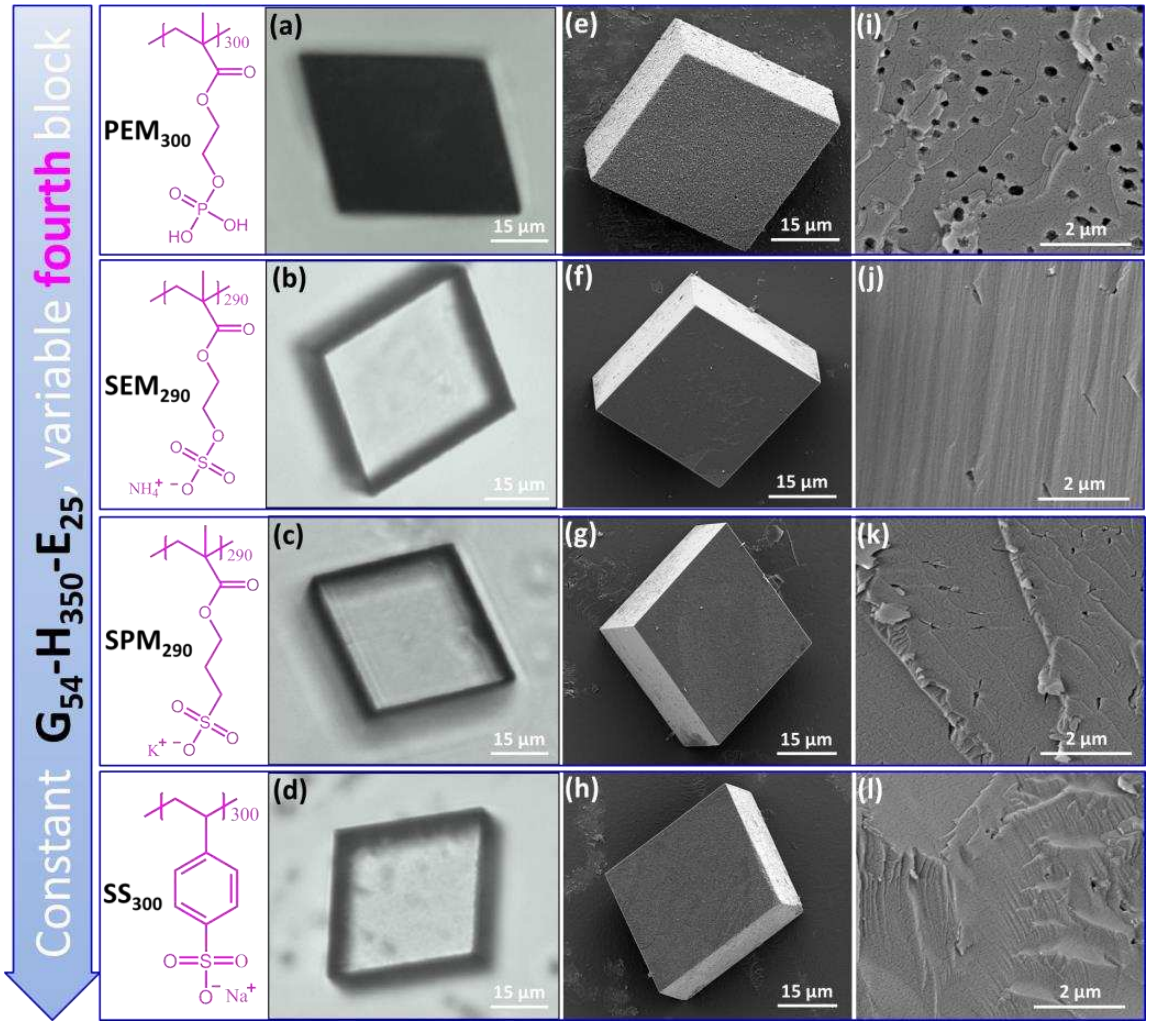

Figure 4. Effect of varying the vesicle surface chemistry on the $CaCO_3$ crystal morphology and extent of occlusion. Chemical structures for the anionic stabilizer block are shown in the first column: poly(2-(phosphonooxy)ethyl methacrylate) (PEM), poly(ammonium 2-sulfatoethyl methacrylate) (SEM), poly(potassium 3-sulfopropyl methacrylate) (SPM), and poly(sodium 4-styrenesulfonate) (SS). (a)-(d) Representative OM images obtained for calcite crystals precipitated in the presence of each type of anionic vesicles; (e)-(h) representative SEM images of the corresponding intact calcite crystals; (i)-(l) representative SEM images showing the internal structure of the same randomly-fractured calcite crystals. In all experiments, calcite crystals were precipitated in the presence of 1.50 mM $CaCl_2$ and 7.77 µM vesicles.

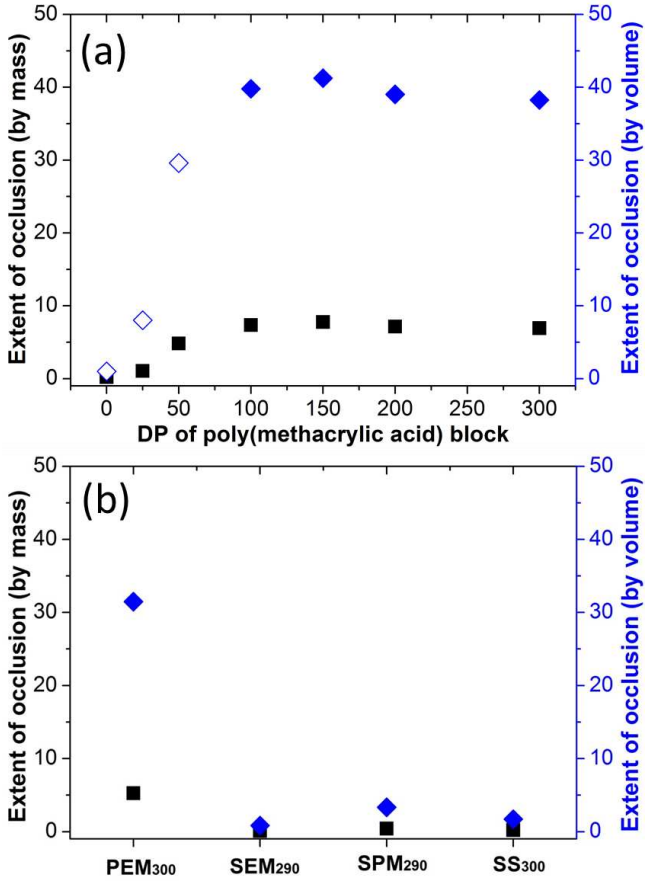

Figure 5. Extent of vesicle occlusion within calcite as a function of either (a) poly(methacrylic acid) block DP or (b) for four alternative anionic stabilizer blocks targeting a fixed DP of 300 (see x axis labels for actual DPs). The extent of vesicle occlusion by % mass (black squares) and by % volume (blue diamonds) was calculated from the TGA data. N.B. Open blue diamonds indicate that these % volume data were calculated by assuming that the overall vesicle dimensions remained unchanged after occlusion.

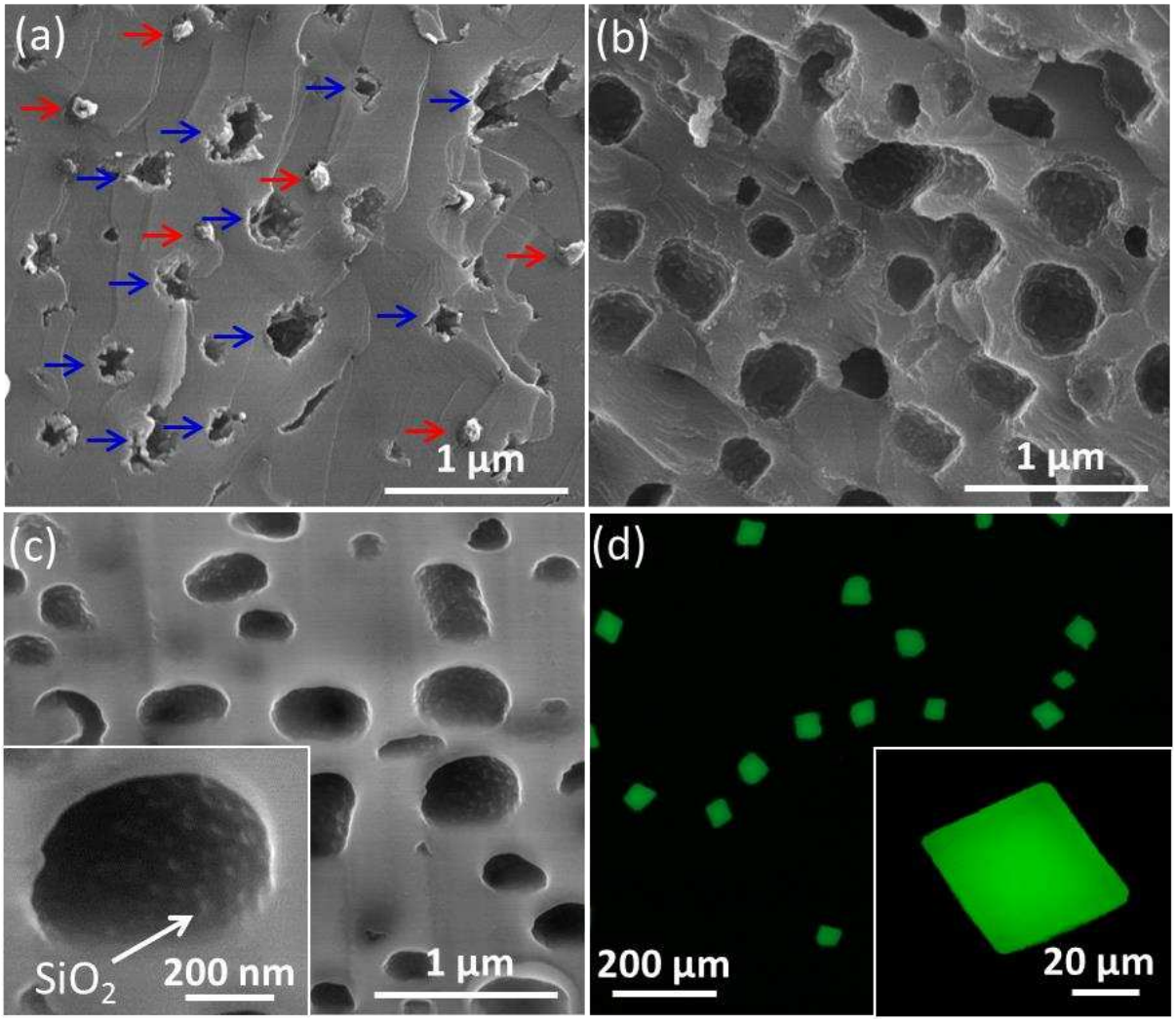

Figure 6. SEM images recorded for cross-sections of calcite crystals prepared in the presence of (a) 7.77 µM silica-loaded G_{54}-H_{350}-E_{25}-MAA_{50} vesicles and (b, c) 7.77 µM silica-loaded G_{54}-H_{350}-E_{25}-MAA_{100} vesicles. [N.B. The cross-section shown in (c) is parallel to the (104) face and was prepared by focused ion beam (FIB) milling]; Inset in (c) is a higher magnification image, showing the presence of silica nanoparticles within this ellipsoidal void. (d) Fluorescence microscopy image recorded for calcite crystals prepared in the presence of 7.77 µM silica-loaded G_{54}-H_{350}-E_{25}-MAA_{100} vesicles. The inset in (d) shows a higher magnification image of a single calcite crystal.

References

1. Berman, A.; Hanson, J.; Leiserowitz, L.; Koetzle, T. F.; Weiner, S.; Addadi, L., Biological-control of crystal texture - a widespread strategy for adapting crystal properties to function. *Science* **1993,** *259*, 776-779.
2. Belcher, A. M.; Wu, X. H.; Christensen, R. J.; Hansma, P. K.; Stucky, G. D.; Morse, D. E., Control of crystal phase switching and orientation by soluble mollusc-shell proteins. *Nature* **1996,** *381*, 56-58.
3. Lowenstam, H. A.; Weiner, S., *On biomineralization*. Oxford University Press: New York: 1989.
4. Mann, S., Biomineralization, Principles and Concepts in Bioinorganic Materials Chemistry. *Oxford University Press: Oxford* **2001**.
5. Xu, A.-W.; Ma, Y.; Cölfen, H., Biomimetic mineralization. *J. Mater. Chem.* **2007,** *17*, 415-449.

6. Aizenberg, J.; Hanson, J.; Koetzle, T.; Weiner, S.; Addadi, L., Control of macromolecule distribution within synthetic and biogenic single calcite crystals. *J. Am. Chem. Soc.* **1997,** *119*, 881-886.
7. Nudelman, F.; Sommerdijk, N. A., Biomineralization as an inspiration for materials chemistry. *Angew. Chem. Int. Ed.* **2012,** *51*, 6582-6596.
8. Metzler, R. A.; Tribello, G. A.; Parrinello, M.; Gilbert, P. U. P. A., Asprich Peptides Are Occluded in Calcite and Permanently Disorder Biomineral Crystals. *J. Am. Chem. Soc.* **2010,** *132*, 11585-11591.
9. Ning, Z.; Gong, X.; Comin, R.; Walters, G.; Fan, F.; Voznyy, O.; Yassitepe, E.; Buin, A.; Hoogland, S.; Sargent, E. H., Quantum-dot-in-perovskite solids. *Nature* **2015,** *523*, 324.
10. Kim, Y.-Y.; Ribeiro, L.; Maillot, F.; Ward, O.; Eichhorn, S. J.; Meldrum, F. C., Bio-Inspired Synthesis and Mechanical Properties of Calcite-Polymer Particle Composites. *Adv. Mater.* **2010,** *22*, 2082-2086.
11. Muñoz-Espí, R.; Jeschke, G.; Lieberwirth, I.; Gómez, C. M.; Wegner, G., ZnO− Latex Hybrids Obtained by Polymer-Controlled Crystallization: A Spectroscopic Investigation. *J. Phys. Chem. B* **2007,** *111*, 697-707.
12. Lu, C. H.; Qi, L. M.; Cong, H. L.; Wang, X. Y.; Yang, J. H.; Yang, L. L.; Zhang, D. Y.; Ma, J. M.; Cao, W. X., Synthesis of calcite single crystals with porous surface by templating of polymer latex particles. *Chem. Mater.* **2005,** *17*, 5218-5224.
13. Li, H.; Xin, H. L.; Muller, D. A.; Estroff, L. A., Visualizing the 3D Internal Structure of Calcite Single Crystals Grown in Agarose Hydrogels. *Science* **2009,** *326*, 1244-1247.
14. Li, H.; Estroff, L. A., Calcite Growth in Hydrogels: Assessing the Mechanism of Polymer-Network Incorporation into Single Crystals. *Adv. Mater.* **2009,** *21*, 470-473.
15. Lu, G.; Li, S.; Guo, Z.; Farha, O. K.; Hauser, B. G.; Qi, X.; Wang, Y.; Wang, X.; Han, S.; Liu, X., Imparting functionality to a metal–organic framework material by controlled nanoparticle encapsulation. *Nat. Chem.* **2012,** *4*, 310-316.
16. Liu, Y.; Zang, H.; Wang, L.; Fu, W.; Yuan, W.; Wu, J.; Jin, X.; Han, J.; Wu, C.; Wang, Y.; Xin, H. L.; Chen, H.; Li, H., Nanoparticles Incorporated inside Single-Crystals: Enhanced Fluorescent Properties. *Chem. Mater.* **2016,** *28*, 7537-7543.
17. Liu, Y.; Yuan, W.; Shi, Y.; Chen, X.; Wang, Y.; Chen, H.; Li, H., Functionalizing Single Crystals: Incorporation of Nanoparticles Inside Gel-Grown Calcite Crystals. *Angew. Chem. Int. Ed.* **2014,** *53*, 4127-4131.
18. Müller, M.; Kaiser, M.; Stachowski, G. M.; Resch-Genger, U.; Gaponik, N.; Eychmüller, A., Photoluminescence quantum yield and matrix-induced luminescence enhancement of colloidal quantum dots embedded in ionic crystals. *Chem. Mater.* **2014,** *26*, 3231-3237.
19. Hu, C.; Ye, T.; Liu, Y.; Ren, J.; Jin, X.; Chen, H.; Li, H., PbI 2 band gap engineering by gel incorporation. *Mater. Chem. Frontiers* **2018,** *2*, 362-368.
20. Otto, T.; Müller, M.; Mundra, P.; Lesnyak, V.; Demir, H. V.; Gaponik, N.; Eychmüller, A., Colloidal Nanocrystals Embedded in Macrocrystals: Robustness, Photostability, and Color Purity. *Nano Lett.* **2012,** *12*, 5348-5354.
21. Kim, Y.-Y.; Ganesan, K.; Yang, P.; Kulak, A. N.; Borukhin, S.; Pechook, S.; Ribeiro, L.; Kroeger, R.; Eichhorn, S. J.; Armes, S. P.; Pokroy, B.; Meldrum, F. C., An artificial biomineral formed by incorporation of copolymer micelles in calcite crystals. *Nat. Mater.* **2011,** *10*, 890-896.
22. Cho, K.-R.; Kim, Y.-Y.; Yang, P.; Cai, W.; Pan, H.; Kulak, A. N.; Lau, J. L.; Kulshreshtha, P.; Armes, S. P.; Meldrum, F. C.; De Yoreo, J. J., Direct observation of mineral-organic composite formation reveals occlusion mechanism. *Nat. Commun.* **2016,** *7*, 10187.
23. Hendley, C. T.; Fielding, L. A.; Jones, E. R.; Ryan, A. J.; Armes, S. P.; Estroff, L. A., Mechanistic Insights into Diblock Copolymer Nanoparticle–Crystal Interactions Revealed via in Situ Atomic Force Microscopy. *J. Am. Chem. Soc.* **2018,** *140*, 7936-7945.
24. Pasteris, J. D.; Freeman, J. J.; Wopenka, B.; Qi, K.; Ma, Q.; Wooley, K. L., With a grain of salt: what halite has to offer to discussions on the origin of life. *Astrobiology* **2006,** *6*, 625-643.

25. Ning, Y.; Fielding, L. A.; Doncom, K. E. B.; Penfold, N. J. W.; Kulak, A. N.; Matsuoka, H.; Armes, S. P., Incorporating Diblock Copolymer Nanoparticles into Calcite Crystals: Do Anionic Carboxylate Groups Alone Ensure Efficient Occlusion? *ACS Macro Lett.* **2016,** *5*, 311-315.
26. Kim, Y.-Y.; Semsarilar, M.; Carloni, J. D.; Cho, K. R.; Kulak, A. N.; Polishchuk, I.; Hendley, C. T.; Smeets, P. J. M.; Fielding, L. A.; Pokroy, B.; Tang, C. C.; Estroff, L. A.; Baker, S. P.; Armes, S. P.; Meldrum, F. C., Structure and Properties of Nanocomposites Formed by the Occlusion of Block Copolymer Worms and Vesicles Within Calcite Crystals. *Adv. Funct. Mater.* **2016,** *26*, 1382-1392.
27. Ning, Y.; Fielding, L. A.; Andrews, T. S.; Growney, D. J.; Armes, S. P., Sulfate-based anionic diblock copolymer nanoparticles for efficient occlusion within zinc oxide. *Nanoscale* **2015,** *7*, 6691-6702.
28. Muñoz-Espí, R.; Qi, Y.; Lieberwirth, I.; Gómez, C. M.; Wegner, G., Surface-functionalized latex particles as controlling agents for the mineralization of zinc oxide in aqueous medium. *Chem. Eur. J.* **2006,** *12*, 118-129.
29. Ning, Y.; Fielding, L. A.; Ratcliffe, L. P. D.; Wang, Y.-W.; Meldrum, F. C.; Armes, S. P., Occlusion of Sulfate-Based Diblock Copolymer Nanoparticles within Calcite: Effect of Varying the Surface Density of Anionic Stabilizer Chains. *J. Am. Chem. Soc.* **2016,** *138*, 11734-11742.
30. Sanson, C.; Schatz, C.; Le Meins, J.-F.; Soum, A.; Thévenot, J.; Garanger, E.; Lecommandoux, S., A simple method to achieve high doxorubicin loading in biodegradable polymersomes. *J. Control. Release* **2010,** *147*, 428-435.
31. Upadhyay, K. K.; Meins, J.-F. L.; Misra, A.; Voisin, P.; Bouchaud, V.; Ibarboure, E.; Schatz, C.; Lecommandoux, S., Biomimetic doxorubicin loaded polymersomes from hyaluronan-block-poly (γ-benzyl glutamate) copolymers. *Biomacromolecules* **2009,** *10*, 2802-2808.
32. Kim, K. T.; Cornelissen, J. J.; Nolte, R. J.; van Hest, J. C., A Polymersome Nanoreactor with Controllable Permeability Induced by Stimuli‐Responsive Block Copolymers. *Adv. Mater.* **2009,** *21*, 2787-2791.
33. Vriezema, D. M.; Garcia, P. M.; Sancho Oltra, N.; Hatzakis, N. S.; Kuiper, S. M.; Nolte, R. J.; Rowan, A. E.; van Hest, J. C., Positional assembly of enzymes in polymersome nanoreactors for cascade reactions. *Angew. Chem.* **2007,** *119*, 7522-7526.
34. Liu, G.; Wang, X.; Hu, J.; Zhang, G.; Liu, S., Self-immolative polymersomes for high-efficiency triggered release and programmed enzymatic reactions. *J. Am. Chem. Soc.* **2014,** *136*, 7492-7497.
35. Li, Y.; Liu, G.; Wang, X.; Hu, J.; Liu, S., Enzyme‐Responsive Polymeric Vesicles for Bacterial‐Strain‐Selective Delivery of Antimicrobial Agents. *Angew. Chem. Int. Ed.* **2016,** *55*, 1760-1764.
36. Lomas, H.; Du, J.; Canton, I.; Madsen, J.; Warren, N.; Armes, S. P.; Lewis, A. L.; Battaglia, G., Efficient Encapsulation of Plasmid DNA in pH-Sensitive PMPC-PDPA Polymersomes: Study of the Effect of PDPA Block Length on Copolymer-DNA Binding Affinity. *Macromol. Biosci.* **2010,** *10*, 513-530.
37. Wang, F.; Xiao, J.; Chen, S.; Sun, H.; Yang, B.; Jiang, J.; Zhou, X.; Du, J., Polymer vesicles: modular platforms for cancer theranostics. *Adv. Mater.* **2018,** *30*, 1705674.
38. Qin, S.; Geng, Y.; Discher, D. E.; Yang, S., Temperature‐Controlled Assembly and Release from Polymer Vesicles of Poly (ethylene oxide)‐block‐poly (N‐isopropylacrylamide). *Adv. Mater.* **2006,** *18*, 2905-2909.
39. Sun, J.-T.; Hong, C.-Y.; Pan, C.-Y., Recent advances in RAFT dispersion polymerization for preparation of block copolymer aggregates. *Polym. Chem.* **2013,** *4*, 873-881.
40. Warren, N. J.; Armes, S. P., Polymerization-Induced Self-Assembly of Block Copolymer Nano-objects via RAFT Aqueous Dispersion Polymerization. *J. Am. Chem. Soc.* **2014,** *136*, 10174-10185.
41. Lowe, A. B., RAFT alcoholic dispersion polymerization with polymerization-induced self-assembly. *Polymer* **2016,** *106*, 161-181.
42. Derry, M. J.; Fielding, L. A.; Armes, S. P., Polymerization-induced self-assembly of block copolymer nanoparticles via RAFT non-aqueous dispersion polymerization. *Prog. Polym. Sci.* **2016,** *52*, 1-18.

43. Chen, S.-L.; Shi, P.-F.; Zhang, W.-Q., In situ synthesis of block copolymer nano-assemblies by polymerization-induced self-assembly under heterogeneous condition. *Chin. J. Polym. Sci.* **2017,** *35*, 455-479.
44. Lesage de la Haye, J.; Zhang, X.; Chaduc, I.; Brunel, F.; Lansalot, M.; D'Agosto, F., The Effect of Hydrophile Topology in RAFT‐Mediated Polymerization‐Induced Self‐Assembly. *Angew. Chem. Int. Ed.* **2016,** *55*, 3739-3743.
45. Wang, X.; An, Z., New Insights into RAFT Dispersion Polymerization‐Induced Self‐Assembly: From Monomer Library, Morphological Control, and Stability to Driving Forces. *Macromol. Rapid Commun.* **2018**, 1800325.
46. Khor, S. Y.; Quinn, J. F.; Whittaker, M. R.; Truong, N. P.; Davis, T. P., Controlling Nanomaterial Size and Shape for Biomedical Applications via Polymerization‐Induced Self‐Assembly. *Macromol. Rapid Commun.* **2018**, 1800438.
47. Le, D.; Keller, D.; Delaittre, G., Reactive and Functional Nanoobject (s) by Polymerization‐Induced Self‐Assembly. *Macromol. Rapid Commun.* **2018**, 1800551.
48. Mable, C. J.; Gibson, R. R.; Prévost, S.; McKenzie, B. E.; Mykhaylyk, O. O.; Armes, S. P., Loading of silica nanoparticles in block copolymer vesicles during polymerization-induced self-assembly: encapsulation efficiency and thermally-triggered release. *J. Am. Chem. Soc.* **2015,** *137*, 16098−16108.
49. Deng, R.; Derry, M. J.; Mable, C. J.; Ning, Y.; Armes, S. P., Using Dynamic Covalent Chemistry To Drive Morphological Transitions: Controlled Release of Encapsulated Nanoparticles from Block Copolymer Vesicles. *J. Am. Chem. Soc.* **2017,** *139*, 7616-7623.
50. Tan, J.; Sun, H.; Yu, M.; Sumerlin, B. S.; Zhang, L., Photo-PISA: Shedding Light on Polymerization-Induced Self-Assembly. *ACS Macro Lett.* **2015,** *4*, 1249-1253.
51. Tan, J.; Liu, D.; Bai, Y.; Huang, C.; Li, X.; He, J.; Xu, Q.; Zhang, L., Enzyme-Assisted Photoinitiated Polymerization-Induced Self-Assembly: An Oxygen-Tolerant Method for Preparing Block Copolymer Nano-Objects in Open Vessels and Multiwell Plates. *Macromolecules* **2017,** *50*, 5798-5806.
52. Blackman, L. D.; Varlas, S.; Arno, M. C.; Fayter, A.; Gibson, M. I.; O'Reilly, R. K., Permeable Protein-Loaded Polymersome Cascade Nanoreactors by Polymerization-Induced Self-Assembly. *ACS Macro Lett.* **2017,** *6*, 1263-1267.
53. Blackman, L. D.; Varlas, S.; Arno, M. C.; Houston, Z. H.; Fletcher, N. L.; Thurecht, K. J.; Hasan, M.; Gibson, M. I.; O'Reilly, R. K., Confinement of Therapeutic Enzymes in Selectively Permeable Polymer Vesicles by Polymerization-Induced Self-Assembly (PISA) Reduces Antibody Binding and Proteolytic Susceptibility. *ACS Centr. Sci.* **2018,** *4*, 718-723.
54. Mable, C. J.; Warren, N. J.; Thompson, K.; Mykhaylyk, O.; Armes, S. P., Framboidal ABC triblock copolymer vesicles: a new class of efficient Pickering emulsifier. *Chem. Sci.* **2015,** *6*, 6179-6188.
55. Mable, C. J.; Fielding, L. A.; Derry, M. J.; Mykhaylyk, O. O.; Chambon, P.; Armes, S. P., Synthesis and pH-responsive dissociation of framboidal ABC triblock copolymer vesicles in aqueous solution. *Chem. Sci.* **2018,** *9*, 1454-1463.
56. Huo, M.; Zeng, M.; Li, D.; Liu, L.; Wei, Y.; Yuan, J., Tailoring the Multicompartment Nanostructures of Fluoro-Containing ABC Triblock Terpolymer Assemblies via Polymerization-Induced Self-Assembly. *Macromolecules* **2017,** *50*, 8212-8220.
57. Huo, M.; Zhang, Y.; Zeng, M.; Liu, L.; Wei, Y.; Yuan, J., Morphology Evolution of Polymeric Assemblies Regulated with Fluoro-Containing Mesogen in Polymerization-Induced Self-Assembly. *Macromolecules* **2017,** *50*, 8192-8201.
58. Zhang, L.; Lu, Q.; Lv, X.; Shen, L.; Zhang, B.; An, Z., In Situ Cross-Linking as a Platform for the Synthesis of Triblock Copolymer Vesicles with Diverse Surface Chemistry and Enhanced Stability via RAFT Dispersion Polymerization. *Macromolecules* **2017,** *50*, 2165-2174.
59. Blanazs, A.; Armes, S. P.; Ryan, A. J., Self-Assembled Block Copolymer Aggregates: From Micelles to Vesicles and their Biological Applications. *Macromol. Rapid Commun.* **2009,** *30*, 267-277.

60. Lovett, J. R.; Warren, N. J.; Ratcliffe, L. P.; Kocik, M. K.; Armes, S. P., pH‐Responsive Non‐Ionic Diblock Copolymers: Ionization of Carboxylic Acid End‐Groups Induces an Order–Order Morphological Transition. *Angew. Chem. Int. Ed.* **2015,** *54*, 1279-1283.
61. Fielding, L. A.; Derry, M. J.; Ladmiral, V.; Rosselgong, J.; Rodrigues, A. M.; Ratcliffe, L. P. D.; Sugihara, S.; Armes, S. P., RAFT dispersion polymerization in non-polar solvents: facile production of block copolymer spheres, worms and vesicles in n-alkanes. *Chem. Sci.* **2013,** *4*, 2081-2087.
62. Li, D.; He, Q.; Li, J., Smart core/shell nanocomposites: intelligent polymers modified gold nanoparticles. *Adv. Colloid Interface Sci.* **2009,** *149*, 28-38.
63. Shan, J.; Tenhu, H., Recent advances in polymer protected gold nanoparticles: synthesis, properties and applications. *Chem. Commun.* **2007**, 4580-4598.
64. Liang, M.; Lin, I. C.; Whittaker, M. R.; Minchin, R. F.; Monteiro, M. J.; Toth, I., Cellular Uptake of Densely Packed Polymer Coatings on Gold Nanoparticles. *Acs Nano* **2010,** *4*, 403-413.
65. Lowe, A. B.; Sumerlin, B. S.; Donovan, M. S.; McCormick, C. L., Facile preparation of transition metal nanoparticles stabilized by well-defined (co) polymers synthesized via aqueous reversible addition-fragmentation chain transfer polymerization. *J. Am. Chem. Soc.* **2002,** *124*, 11562-11563.
66. Addadi, L.; Moradian, J.; Shay, E.; Maroudas, N.; Weiner, S., A chemical model for the cooperation of sulfates and carboxylates in calcite crystal nucleation: relevance to biomineralization. *Proc. Natl. Acad. Sci.* **1987,** *84*, 2732-2736.
67. Aizenberg, J.; Black, A. J.; Whitesides, G. M., Control of crystal nucleation by patterned self-assembled monolayers. *Nature* **1999,** *398*, 495.
68. Orme, C. A.; Noy, A.; Wierzbicki, A.; McBride, M. T.; Grantham, M.; Teng, H. H.; Dove, P. M.; DeYoreo, J. J., Formation of chiral morphologies through selective binding of amino acids to calcite surface steps. *Nature* **2001,** *411*, 775-779.
69. Teng, H. H.; Dove, P. M.; Orme, C. A.; De Yoreo, J. J., Thermodynamics of calcite growth: Baseline for understanding biomineral formation. *Science* **1998,** *282*, 724-727.
70. Wehrmeister, U.; Soldati, A. L.; Jacob, D. E.; Haeger, T.; Hofmeister, W., Raman spectroscopy of synthetic, geological and biological vaterite: a Raman spectroscopic study. *J. Raman Spectrosc.* **2010,** *41*, 193-201.
71. Ning, Y.; Whitaker, D. J.; Mable, C. J.; Derry, M. J.; Penfold, N. J. W.; Kulak, A. N.; Green, D. C.; Meldrum, F. C.; Armes, S. P., Anionic block copolymer vesicles act as Trojan horses to enable efficient occlusion of guest species into host calcite crystals. *Chem. Sci.* **2018,** *9*, 8396-8401.
72. Kulak, A. N.; Semsarilar, M.; Kim, Y.-Y.; Ihli, J.; Fielding, L. A.; Cespedes, O.; Armes, S. P.; Meldrum, F. C., One-pot synthesis of an inorganic heterostructure: uniform occlusion of magnetite nanoparticles within calcite single crystals. *Chem. Sci.* **2014,** *5*, 738-743.
73. Dean, J. A., *Lange's handbook of chemistry*. New york; London: McGraw-Hill, Inc.: 1999.
74. Warren, N. J.; Mykhaylyk, O. O.; Ryan, A. J.; Williams, M.; Doussineau, T.; Dugourd, P.; Antoine, R.; Portale, G.; Armes, S. P., Testing the Vesicular Morphology to Destruction: Birth and Death of Diblock Copolymer Vesicles Prepared via Polymerization-Induced Self-Assembly. *J. Am. Chem. Soc.* **2015,** *137*, 1929-1937.

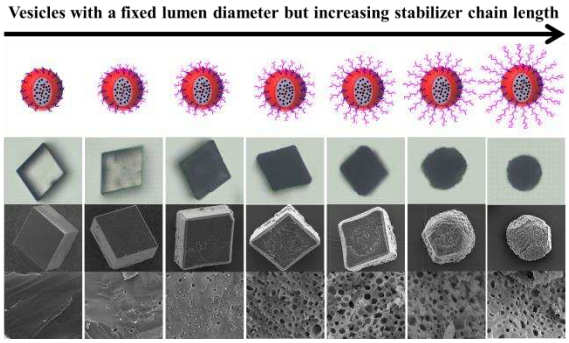
Vesicles with a fixed lumen diameter but increasing stabilizer chain length